ELSEVIER

Journal of Alloys and Compounds 404–406 (2005) 617–620

Journal of ALLOYS AND COMPOUNDS

www.elsevier.com/locate/jallcom

Transmission electron microscopy of hydrogen effects in internally oxidized palladium–chromium alloys

G. Gouthama[a], R. Balasubramaniam[a,*], D. Wang[b], T.B. Flanagan[b]

[a] *Department of Materials and Metallurgical Engineering, Indian Institute of Technology, Kanpur 208016, India*
[b] *Department of Chemistry, University of Vermont, Burlington, VT 05425, USA*

Received 12 August 2004; received in revised form 16 March 2005; accepted 21 March 2005
Available online 7 July 2005

Abstract

Hydrogen has been successfully used as a probe to characterize internally oxidized Pd alloys. Hydrogen isotherms indicated enhanced hydrogen solubilities in the dilute phase region for internally oxidized Pd–Cr alloys. The microstructures of internally oxidized Pd–Cr alloys have been studied by transmission electron microscopy. In the case of IOed $Pd_{0.98}Cr_{0.02}$ and $Pd_{0.96}Cr_{0.04}$ alloys, TEM revealed large chromia particles, in the size range 100–200 nm, on high angle grain boundaries. The size of loops and precipitates was larger and their number density smaller compared to those present in the grain interior where there was a uniform distribution of precipitates and dislocation loops throughout the matrix. After hydrogen cycling the internally oxidized $Pd_{0.96}Cr_{0.04}$ alloy, a high density of dislocations, in the form of dislocation cells, and sub-grain formation were observed. The microstructures were indicative of the high degree of cyclic stress induced during the hydrogen cycling process. The hydrogen solubility enhancement in internally oxidized Pd–Cr alloys have been co-related with the presence of dislocation loops.

Keywords: Internal oxidation; Pd–Cr alloys; Transmission electron microscopy; Hydrogen isotherms

1. Introduction

Upon high temperature exposure (≥973 K) of a Pd–M alloy to an oxidizing environment, oxygen dissociates at the surface and O atoms dissolve and diffuse to internally oxidize M, where M is a solute more easily oxidizable than Pd, to produce oxide precipitates in a matrix of pure Pd. This is an example of internal oxidation (IO) [1]. As these precipitates are generally nano-sized, the material produced after IO can be termed as nano-oxide dispersed composites. Hydrogen can be used as a probe to help characterize these composites [2]. Hydrogen behavior in internally oxidized systems can be monitored either by electrochemical [2] or gas phase [3] methods. Hydrogen behavior in several internally oxidized Pd–Al, Pd–Rh, Pd–Ni, Pd–Fe and Pd–Mo alloys have been studied [4–6].

The objective of the project is to study internally oxidized Pd–Cr alloys and the effect of hydriding and dehydriding using electron microscopy because the dilute phase hydrogen solubility enhancements in internally oxidized Pd–Cr alloy are much greater than in other systems. The microstructures were characterized to understand dilute phase solubility enhancements in internally oxidized Pd–Cr alloys.

2. Experimental

The Pd–Cr alloys were prepared by arc-melting the pure elements under argon. The buttons were flipped and re-melted several times. They were then annealed in vacuo for 3 days at 1133 K, rolled into foils and then re-annealed for 2 days at 1133 K. The alloys were then oxidized in air at several different temperatures from 973 to 1273 K for various lengths of time. They were quenched after internal oxidation in order to avoid the oxidation of Pd. After internal oxidation, weight gain measurements indicate that the internal oxide possesses a stoichiometry close to Cr_2O_3.

The microstructures after IO and hydrogen interactions were characterized in a JEOL 2000 FX transmission electron

* Corresponding author.
E-mail address: bala@iitk.ac.in (R. Balasubramaniam).

0925-8388/$ – see front matter © 2005 Elsevier B.V. All rights reserved.
doi:10.1016/j.jallcom.2005.03.100

microscope (TEM). The strips were first thinned to about 0.5 mm thickness and 3 mm diameter discs were punched out from the strips. Thin foils suitable for TEM were prepared by jet polishing with a solution containing 77% acetic acid and 23% perchloric acid. The surfaces of the IOed alloys were also observed in a JEOL JSM840 scanning electron microscope.

3. Results and discussions

3.1. Hydrogen isotherms

The dilute phase hydrogen solubilities (323 K) of the internally oxidized (1098 K, 72 h) $Pd_{0.97}Cr_{0.03}$ alloy are presented in Fig. 1. The dashed line indicates initial solubilities in pure Pd. The filled symbols are the repeat solubilities without hydriding, while the arrow indicates the solubilities after cycling. There is a positive intercept of the initial isotherm for the IOed alloy on the H/M axis and this is due to strong irreversible hydrogen trapping at the oxide-matrix interfaces [7]. There is a significant enhancement in the dilute phase hydrogen solubility in the case of the IOed alloy, which is clearly noted in the repeat solubility isotherm where the irreversible trapping is not observed because these traps have been filled up during the initial run. Upon cycling the alloy, the irreversible traps re-appear and, moreover, an additional solubility enhancement is also observed on cycling. The hydrogen solubility enhancements were theoretically estimated in the Pd–Cr system based on calculation of thermal stresses in the matrix, as per the procedure adopted earlier for the Pd–Al system [3] and they were not significantly greater that that predicted for the Pd–Al system. Therefore, the probable reasons for the enhancement in dilute phase hydrogen solubilities, both before and after cycling, were explored by characterizing the microstructures.

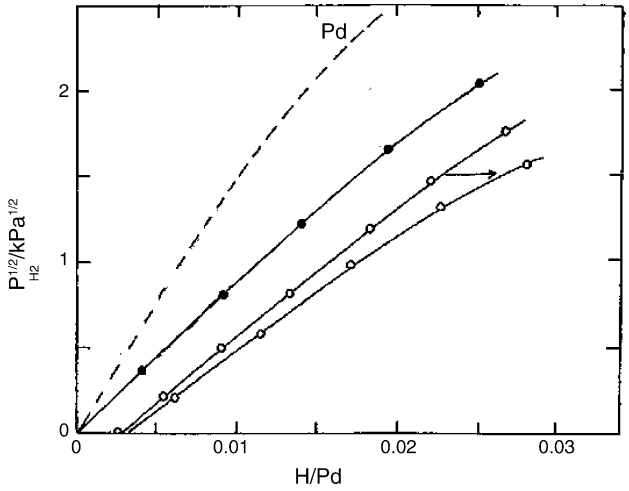

Fig. 1. Dilute phase hydrogen solubilities (323 K) for internally oxidized (1098 K, 72 h) $Pd_{0.97}Cr_{0.03}$ alloy. The dashed line indicates solubilities in pure Pd. The filled symbols are the repeat solubilities without hydriding, while the arrows indicate the solubilities after cycling.

3.2. Microscopy

SEM observations of the surface of internally oxidized Pd–Cr showed thermal grooves formed due to dislocation motion at high temperature. At some locations, Pd nodules could be seen. Pores were also observed on the grain boundaries, leading to a honey-comb-like appearance of the grain walls within the cracked grain boundaries. The internally oxidized samples were cracked and the cracks were generally intergranular in nature. Upon hydrogen cycling, the severity of intergranular cracking increased. The enhanced rates of hydrogen uptake (and discharge) in these internally oxidized systems must be related to these features observed on the surface [8,9].

The internally oxidized Pd–Cr alloys were observed by TEM. TEM images revealed the presence of precipitates, which had formed as a result of internal oxidation (Fig. 2). The precipitates were not visible in SEM micrographs because of their small size. Analysis of electron diffraction patterns of the precipitate proved that they were chromia.

A TEM micrograph (Fig. 2) shows a region close to the grain boundary of a sample of $Pd_{0.98}Cr_{0.02}$ after internal oxidation. On high angle grain boundaries, large chromia particles in the size range 100–200 nm are evident. There is a uniform distribution of chromia precipitates as well as dislocation loops (marked by L) through out the matrix. Close to the grain boundary the size of the loops and the precipitate are coarser in size and fewer in number as compared to those present in the grain interior. The precipitate free zone close to the grain boundary is also evident. This is due to the solute depletion in this region in forming the large grain boundary precipitates. The dislocation loop depletion in this region

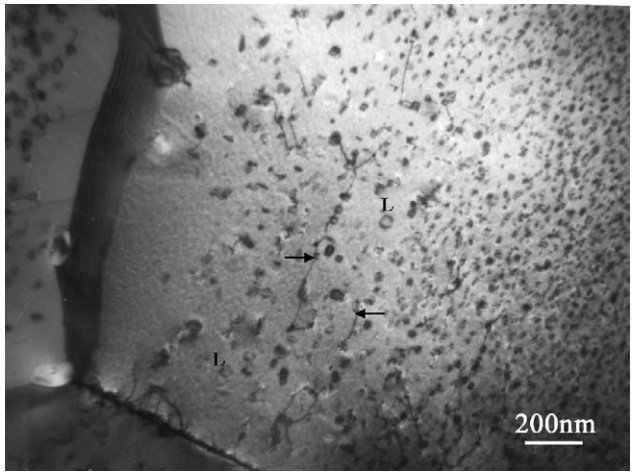

Fig. 2. Transmission electron micrograph illustrating the distribution of the chromia particles and the dislocation loops in the internally oxidized $Pd_{0.98}Cr_{0.02}$ sample.

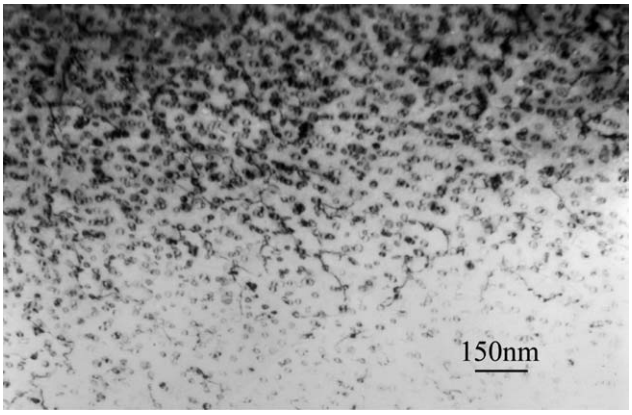

Fig. 3. Transmission electron micrograph illustrating the distribution of the chromia particles and the dislocation loops in the internally oxidized $Pd_{0.96}Cr_{0.04}$ sample.

is caused by the vacancy depletion in this region. Some dislocations are also clearly evident. Some precipitates that are pinning the dislocations are arrowed in Fig. 2.

TEM micrograph of Fig. 3 shows the distribution of chromia precipitates and the loops in the grain interior for $Pd_{0.96}Cr_{0.04}$ after internal oxidation. It is difficult to distinguish between the chromia precipitates and the dislocation loops. The chromia particles look a little darker in contrast and also are distinguishable from the dislocation tangles associated with them in several locations. The dislocation loops show the line of no contrast and exhibit the typical 'coffee bean' contrast. The dislocation loop number density is many fold higher (five times or more) than the chromia density. The size of dislocation loops is in the range 10–15 nm. The chromia particles size ranges from 5 to 15 nm within the grains. Dislocation loops were not observed in the case of other internally oxidized Pd alloys [4,6].

Microstructural details after hydrogen cycling the $Pd_{0.96}Cr_{0.04}$ alloy after internal oxidation are seen in Fig. 4. A high density of dislocations is readily evident. Dislocation cell formation and sub-grain formation are noticed. The right top corner is a region close to the grain boundary. The microstructure is typical of highly deformed or cyclically loaded sample. This is indicative of the high degree of stress induced during the hydrogen cycling process.

The enhancement in the dilute phase hydrogen solubilities can be related to the presence of dislocation loops, which can act as reversible traps for hydrogen. With higher amounts of chromia precipitates, a larger number of dislocation loops form because these are punched out at the temperature of internal oxidation to accommodate the transformation stresses. Therefore, higher solubility enhancements are anticipated for internally oxidized Pd–Cr alloys with higher Cr contents. On hydrogen cycling, there is an increase in the dislocation density of the samples and this can explain the enhancement in hydrogen solubilities on cycling, as has been explained in the case of pure Pd [10].

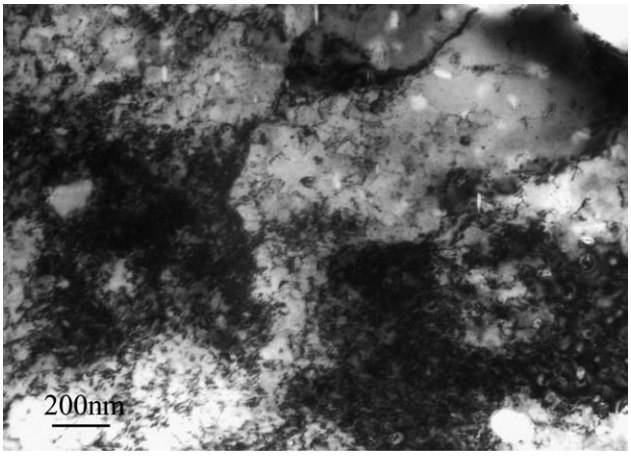

Fig. 4. Micrographs showing the microstructure of the internal oxidized $Pd_{0.96}Cr_{0.04}$ alloy after hydrogen cycling. Dislocation cell formation due to the hydrogen cycling is evident.

4. Conclusions

The microstructures of internally oxidized Pd–Cr alloys have been studied by electron microscopy. Hydrogen isotherms indicate enhanced hydrogen solubilities in the dilute phase region for internally oxidized Pd–Cr alloys. Scanning electron microscopy revealed intergranular cracking after internal oxidation, which was accelerated on hydrogen cycling. Electron diffraction in the transmission electron microscope (TEM) confirmed that the precipitate that forms on internal oxidation of Pd–Cr alloys is chromia. In the case of internally oxidized $Pd_{0.98}Cr_{0.02}$ and $Pd_{0.96}Cr_{0.04}$ alloys, TEM revealed large chromia particles, in the range 100–200 nm located on high angle grain boundaries. There was a uniform distribution of dislocation loops all over the matrix. The size of loops and precipitates was larger and their number density smaller in the grain boundaries than in the grain interior. After hydrogen cycling the internally oxidized $Pd_{0.96}Cr_{0.04}$ alloy, a high density of dislocations, in the form of dislocation cells and sub-grain formation, were noticed. The hydrogen solubility enhancements in the internally oxidized Pd–Cr alloys have been related to the presence of dislocation loops, while the enhancements on cycling have been related to the generation of dislocations during the process of hydriding and dehydriding.

References

[1] J. Meijering, in: H. Herman (Ed.), Advances in Materials Research, vol. 5, Wiley, New York, 1971, p. 1.
[2] X. Huang, W. Mader, J. Eastman, R. Kirchheim, Scripta Met. 22 (1988) 1109.
[3] H. Noh, T.B. Flanagan, R. Balasubramaniam, J. Eastman, Scripta Mater. 34 (1996) 863.
[4] R. Balasubramaniam, H. Noh, T.B. Flanagan, Y. Sakamoto, Acta Mater. 45 (1997) 1725.

[5] W. Zhang, S. Luo, D. Wang, T.B. Flanagan, R. Balasubramaniam, J. Alloys Compd. 330–332 (2002) 607.
[6] H. Noh, D. Wang, S. Luo, T.B. Flanagan, R. Balasubramaniam, Y. Sakamoto, J. Phys. Chem. B 108 (2004) 310–319.
[7] D. Wang, H. Noh, S. Luo, T.B. Flanagan, J.D. Clewley, R. Balasubramaniam, J. Alloys Compd. 339 (2002) 76–89.
[8] R. Balasubramaniam, R. Kirchheim, D. Wang, T.B. Flanagan, J. Alloys Compd. 293–295 (1999) 306–309.
[9] D. Wang, J.D. Clewley, T.B. Flanagan, R. Balasubramaniam, K.L. Shanahan, J. Alloys Compd. 298 (2000) 261–273.
[10] J.F. Lynch, J.D. Clewley, T. Curran, T.B. Flanagan, J. Less-Common Met. 55 (1977) 153.